Revista Mexicana de Física
ISSN: 0035-001X
rmf@ciencias.unam.mx
Sociedad Mexicana de Física A.C.
México

Herrera-Suárez, H.J.; Rubio-Ponce, A.; Olguín, D.
Electronic band structure of platinum low-index surfaces: an ab initio and tight-binding study. II
Revista Mexicana de Física, vol. 58, núm. 1, febrero, 2012, pp. 46-54
Sociedad Mexicana de Física A.C.
Distrito Federal, México

Electronic band structure of platinum low–index surfaces: an *ab initio* and tight–binding study. II

H.J. Herrera-Suárez
Universidad de Ibagué, Facultad de Ciencias Naturales y Matemáticas, Colombia, Carrera 22 Calle 67 Barrio Ambalá.

A. Rubio–Ponce
Departamento de Ciencias Básicas, Universidad Autónoma Metropolitana–Azcapotzalco, Av. San Pablo 180, México, D.F. 02200, México.

D. Olguín
Departamento de Física, Centro de Investigación y de Estudios Avanzados del Instituto Politécnico Nacional, Apartado Postal 14740, México, D.F. 07300, México.

Recibido el 30 de agosto de 2011; aceptado el 25 de noviembre de 2011

We present the calculated electronic band structure of ideal Pt(100) and Pt(110) surface by using density functional theory and the empirical tight–binding method. A detailed discussion of the surface– and resonance–states is given. It is shown that the calculated surface– and resonance–states of ideal Pt(100) surfaces agree very well with the available experimental data. For Pt(110), some of the surface– and resonance–states are characteristic of the low symmetry of the surface and are identified as being independent of surface reconstruction effects. As in the previous paper, the density functional calculations were performed using the full potential linearized augmented plane wave method, and the empirical calculations were performed using the tight–binding method and Surface Green's Function Matching Method.

Keywords: *Ab initio* calculations; surface states; resonance states; tight–binding calculations; metal surfaces.

Presentamos el cálculo de la estructura electrónica de bandas de la superficie ideal del Pt(100) y Pt(110). El cálculo se realizó utilizando la teoría del funcional de la densidad y el método de enlace fuerte. Como resultado de nuestro cálculo presentamos una discusión detallada de los estados resonantes y los estados de superficie. Para la superficie ideal del Pt(100) mostramos que tanto los estados de superficie como los estados resonantes concuerdan aceptablemente con datos experimentales. Para el caso de Pt(110) hallamos que los estados resonantes y de superficie característicos de la dimensionalidad de la superficie, son independientes de la reconstrucción y se reproducen aceptablemente en nuestro cálculo. Al igual que en el trabajo anterior, utilizamos la teoría del funcional de la densidad con el método de ondas planas aumentadas, mientras que los cálculos empíricos se han hecho utilizando el método de enlace fuerte junto con el método de empalme de las funciones de Green.

Descriptores: Cálculo *Ab initio*; estados de superficie; estados resonantes; cálculos de enlace fuerte; superficies metálicas.

PACS: 73.20.At; 71.15.Ap; 71.15.Mb

1. Introduction

A detailed understanding of the surface electronic band structure is useful for predicting the equilibrium shape of a mesoscopic crystal and is important for understanding a wide variety of phenomena such as catalysis [1], surface reactivity, growth, the creation of steps and kinks on surfaces, and physisorption [2,3]. To obtain this detailed knowledge, experimental data can be complemented with calculations. Two primary type of calculations are used in practice. The first kind includes empirical and semi–empirical calculations, of which the empirical tight–binding (ETB) method is one of the most transparent and widely used methods. However, there are also first–principle calculations. At present, first–principle calculations from approximate methods such as density functional theory (DFT) are widely used, and their predictions are widely accepted by the scientific community.

In a previous paper we have discussed our calculations for the Pt(111) surface [4]. In this work we present the continuation of our study of the Pt low–index surfaces. In this context, the electronic band structures of ideal Pt(100) and Pt(110) surfaces are calculated using a DFT method, ETB calculations of the studied surfaces are also presented for comparison. It was found that the two methods yield similar results.

The Pt(100) surface is usually studied in the (1×1) and (5×1) phases. The unreconstructed (1×1) phase is metastable, whereas the reconstructed (5×1) phase is obtained after the sample is annealed at 400 K [5-7]. In the present work, the reported surface– and resonance–states of the metastable (1×1) phase [5] are accurately reproduced. Also, a controversial surface–state that was recently reported by Subaran *et al.* [6], and that was not observed in previous reports, is properly identified in our calculations.

It is established that the Pt(110) surface exhibits the so–called (1×2) missing row reconstruction, whereas the (1×1) phase is metastable [8-11]. In this work, however, the calculation was performed on an ideal Pt(110) surface. Although we did not find experimental data related with this phase, for completeness, we will discuss our results and will qualitatively compare them with previous experimental data on

the (1×2) missing row phase [8,10]. The calculations reveal several surface– and resonance–states that are reported to be a characteristic of the low symmetry of the surface. These states are identified as being independent of surface reconstruction effects, and these facts support our proposal to compute the electronic band structure of this surface.

The rest of the paper is organized as follows: In Sec. 2, the essentials of the calculation methods are given. Section 3 contains our results, a detailed discussion of our findings is given in Subsec. 3.2 and 3.3. A comparison of our results with the ETB calculations is also presented in these subsections. Section 4 summarizes our work.

2. Computational methods

2.1. The FLAPW Method

The DFT calculations were performed using the full potential linearized augmented plane wave method (FLAPW) method as implemented in the Wien2k code [12]. In this method, the wave functions, the charge density, and the potential are expanded in spherical harmonics within non–overlapping muffin–tin spheres, and plane waves are used in the remaining interstitial region of the unit cell. In the code, the core and valence states are handled differently. Core states are treated with a multi–configuration relativistic Dirac–Fock approach, whereas valence states are treated with a scalar relativistic approach. The exchange–correlation energy was calculated using the local–spin–density approximation (LSDA) because the LSDA works better than the alternative gradient–generalized approximation (GGA) when computing several properties of metal surfaces [3,13]. In the calculations, a step analysis was carefully performed to ensure the convergence of the total energy in terms of the variational cutoff–energy parameter. At the same time, an appropriate set of k–points was used to compute the total energy. The atomic electronic configuration of Pt used in the calculations was as follows: [Xe] $4f^{14}$, $5d^{9}$, $6s^{1}$. The $5p$ orbitals were included by using the local orbital extension of the FLAPW method [12].

By computing the total energy of a primitive cell as a function of the volume and fitting the data to the third order Birch–Murnaghan [14] equation of state, the lattice parameter $a_{\rm theo}$=3.9176 Å, the bulk modulus B=323.5510 GPa, and the pressure derivative of the bulk module B'=4.8226 for the primitive face–centered cubic (fcc) Pt lattice were found (the GGA–calculated value for the bulk modulus and its pressure derivative were B=263.7040 GPa and B'=5.9372, respectively, and the calculated lattice parameter was a=3.9883 Å, whereas the experimental value of the lattice parameter is $a_{\rm exp}$=3.9231 Å [15], and that of the bulk modulus is $B = 278$ GPa [16]).

To minimize the total energy of the Pt(100) surface, a supercell with 15–atomic layers and 9–vacuum layers was used, whereas a supercell of 21–atomic layers and 13–vacuum layers was used for the Pt(110) surface. The variational parameters used for the two studied surfaces were $R_{\rm kmax} = 9$ Ry and $G_{\rm max} = 14$. The total energy of the Pt(100) surface was minimized using a set of 91 $k-$points in the irreducible portion of the BZ, equivalent to a (25×25×1) Monkhorst–Pack [17] grid in the unit cell. For the Pt(110) surface, the total energy was minimized using a set of 88 $k-$points in the irreducible portion of the BZ, equivalent to a $(22 \times 16 \times 1)$ Monkhorst–Pack [17] grid. Finally, the total energy was converged with a resolution better than 0.0001 Ry.

2.2. The empirical Tight–Binding method

The ETB calculations were done using the scheme proposed by Slater–Koster [18] in conjunction with the Surface Green–Function–Matching (SFGM) method [20]. We use the ETB method with a minimal orthogonal basis of nine atomic orbitals, sp^3d^5, per atom in the unit cell and in the approach we have included first nearest and next nearest neighbors. The parameters of the model are those used by Papaconstantopoulos, as it is known that these parameters properly reproduce the bulk electronic properties of Pt when used in DFT calculations [19]. Since the SGFM method takes into account the perturbation caused by the surface exactly, at least in principle, we can use the bulk tight–binding parameters (TBP) [20]. This does not mean that we are using the same TBP for the surface and the bulk. Their difference is taken into account through the matching of the Green's functions. We used the method in the form cast by García–Moliner and Velasco [20]. They make use of the transfer matrix approach first introduced by Falicov and Yndurain [21]. This approach became very useful due to the quickly converging algorithms of López–Sancho *et al.* [22]. Following the suggestions of these authors, the algorithms for all transfer matrices needed to deal with these systems can be found in a straightforward way. This method has been employed successfully for the study of the electronic properties of semiconductor surfaces [23,24] and transition metals [25-28].

When a surface is introduced, and thus the system becomes semi–infinite, the boundary conditions require that the wave function vanishes at the surface. These new boundary conditions modify the energy spectrum and cause the occurrence of new states. These new states exist only in the few atomic layers close to the surface atomic layer. The wave function of these states decays exponentially from the surface into the bulk. All these effects, that are a consequence of the introduction of a surface into an infinite periodic medium, can be better described within the surface Green's function formalism.

We introduce the surface Green's functions by using the known tight–binding formulae [20]:

$$G_s^{-1} = (\varepsilon I - H_{00}) - H_{01}T \tag{1}$$

$$G_b^{-1} = G_s^{-1} - H_{10}\widetilde{T} \tag{2}$$

Where G_s^{-1} (G_b^{-1}) is the surface (bulk) projected Green's function, and H_{00}, H_{01}, and H_{10} are the surface tight–binding Hamiltonians, and T and $\tilde{T}$ are the transfer matrices.

The way in which the tight–binding Hamiltonians and the SGFM method are related is described in detail in Refs. 20, 23, 24, and 29. From the knowledge of the Green's function, the surface states and the resonance states can be calculated from the poles of the real part of the corresponding Green's function.

3. Results and discussion

3.1. Density of states

As in the Pt(111) [4] case, and to check the accuracy of the electronic properties calculated from the supercell approach, the calculated bulk density of states (DOS) is compared with the DOS projected onto the central atomic layers of the different supercells. It should be noted that, in this approach, the DOS projected onto the central atomic layer must be similar to the calculated bulk DOS. Figure 1 shows that this is the case. In the figure, the calculated bulk DOS is shown as a solid line, the calculated DOS projected onto the central atomic layer is presented as a dotted line, and the calculated DOS projected onto the outer atomic layer is presented as a broken line. In the upper panel, the partial bulk–DOS due to the Pt–$5d$ orbitals is also shown. The figure shows that in the energy range from approximately –7.0 eV to 0.5 eV, the main contribution to the bulk DOS is obtained from the Pt–$5d$ electrons. This symmetry composition will be reflected on the symmetry of the obtained surface electronic band structure, as we will show later. The upper panel shows the calculated DOS of Pt(100) and the lower panel shows the results for Pt(110). In the figures, the zero of the energy axis represents the Fermi level (E_F). The figure shows that below E_F, the DOS projected onto the central layer (broken line) properly reproduces the main features of the bulk DOS (solid line) for each studied surface. The bulk DOS exhibits four main peaks that are accurately reproduced by the DOS projected onto the central atomic layer. The same is true for the width and energy of the main peak. The small observed differences are related to the shape of the main peaks. Above E_F, Fig. 1 shows that the DOS projected onto the central layer properly reproduces the bulk DOS up to 6.0 eV, at which point some differences between the two calculations were observed.

On the other hand, it is clear from Fig. 1 that the calculated DOS projected onto the outer atomic layer is significantly different from the bulk DOS. There are important features obtained from the projected surface DOS; these features were obtained below and above E_F but were not obtained for the bulk DOS. Information about the surface– and resonance–states will be found from these differences. Below E_F, resonance–states are expected to be obtained, mainly because these energies represent the continuum of the projected bulk bands, and few energy gaps exist at these energy values. The surface–states will be obtained above E_F because energy gaps are more frequently observed at these energies.

The comparison of the calculated bulk DOS using the ETB–SGFM and the DFT methods is shown in the inset of each figure. As can be observed the calculated DOS using both methods are quite similar, mainly for energies below E_F. From these facts, it will be shown that the found surface electronic band structure is also quite similar in both calculations.

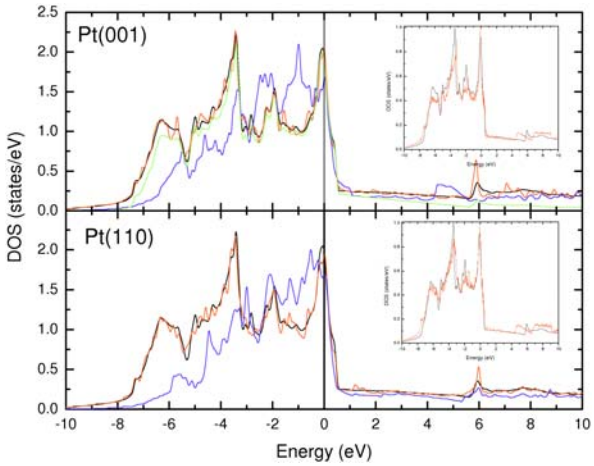

FIGURE 1. (Color online) Calculated DOS of the different Pt–surfaces studied in this work. The bulk DOS is presented as a black line, the DOS projected onto the central atomic layer is presented as a red line, and the DOS projected on the surface atomic layer is presented as a blue line. For comparison, the partial Pt–$5d$ contribution to the DOS is also presented as a green line (upper panel). The inset in each panel shows the comparison of the bulk DOS calculated using the FLAPW (black line) method and the bulk projected DOS calculated using the SGFM–ETB (red line) method.

In the rest of the section, the surface– and resonance–states found in our study will be discussed. First, the DFT calculations will be shown, then the calculated states of each studied surface will be shown and compared with experimental data. Finally, the ETB calculations, the DFT calculations, and the experimental data will be compared.

We have calculated the electronic band structure of ideal surfaces. The surface–states (SSs) and the resonance–states (RSs) are electronic states found at the surfaces of the materials. These states are characterized by energy bands that are not degenerate with the bulk energy bands. These states only exist in the forbidden energy gaps. At energies for which the surface and bulk states are degenerate (*i.e.*, where the surface states and the bulk states mix), a surface resonance forms. Such states can propagate into the bulk, similar to Bloch waves, and can retain enhanced amplitudes near the surface.

The calculated SSs and RSs, as well as the projected bulk bands (pbbs) of the studied surfaces, are shown in Figs. 2 and 3. The results shown in these figures should be interpreted as follows: The pbbs are a fingerprint of each surface and are represented by small black dots. In principle, these pbbs should be a continuum for a enormous supercell (*i.e.*, a semi–infinite medium); however, because of the finite size of the employed supercell, a series of dotted lines "representing" the continuum is observed. In the figures, red points

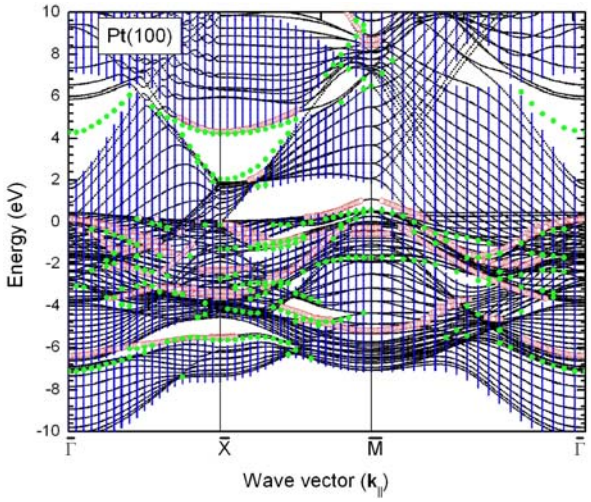

FIGURE 2. (Color online) Projected bulk bands of Pt(100). Black dots represent the DFT calculated pbbs. Red dots represent the SSs or the RSs if the states are located in a local energy gap or in the continuum bulk bands, respectively. The blue dots represent the pbbs calculated by the ETB method, and the SSs and RSs are represented by green dots.

represent the SSs and RSs. Some local energy gaps can be observed in the pbbs. The SSs are expected in these local gaps, whereas the RSs must be observed in the continuum of the pbbs.

3.2. Platinum(100)

Figure 2 shows the calculated DFT pbbs as well as the SSs and RSs for Pt(100). Table I shows the wavefunction compositions of the different SSs and RSs.

For this surface, at the $\bar{X}$ point, an SS was found approximately 4.3 eV above E_F. An RS was also found at the $\bar{M}$ point at energies that range from 9.0 eV to 10.0 eV, as seen in Fig. 2. These states are supported by the calculated DOS projected onto the surface as noted in Fig. 1. According to the DFT calculations, the wavefunctions of these states have the symmetries of the $s, d_{x^2+y^2}$ and d_{xy} orbitals, respectively.

However, as can be observed in Fig. 2, a number of SSs and RSs were obtained at energies below E_F. According to the convention for a resonance state given above, an RS was obtained at lower energies, approximately -6.4 eV below E_F. The state seems to begin at the $\bar{M}-\bar{\Gamma}$ interval, continues to the $\bar{\Gamma}-\bar{X}$ interval, and then goes to an SS located in the lower local gap at $\bar{X}$. The state shows little dispersion as a function of $\mathbf{k}_{||}$. The wavefunction composition of this state has the $s, d_{x^2+y^2}$ symmetry.

An RS was obtained at energies of approximately -3.6 eV in the $\bar{\Gamma}-\bar{X}$ interval and seems to have an oscillatory shape. That is, the state seems to extend throughout the surface Brillouin zone (SBZ), crossing the $\bar{X}$–point at -3.6 eV, then crossing the $\bar{M}$–point at -0.2 eV, and finally ending at -3.6 eV in the middle of the $\bar{M}-\bar{\Gamma}$ interval. Although the state seems to be discontinuous in its trajectory, this could be a consequence of the numerical accuracy; the state should be a single band crossing the entire SBZ. A similar pattern was obtained for the Pt(111) surface [4]. The wavefunction composition of this RS has the $d_{x^2+y^2}, d_{xz}$ symmetry.

Similar comments are appropriate for the RS that begins at -2.1 eV in the $\bar{\Gamma}-\bar{X}$ interval and seems to continue through the $\bar{X}$–point before going through the $\bar{M}$–point and mixing with the previously discussed RS. This state finally ends at the $\bar{\Gamma}$–point once again. Although it is difficult to establish a unique pattern for these RSs, it could be possible that they represent one band that crosses the entire SBZ. The wavefunction compositions found for these RSs are d_{xz}, d_{z^2}, d_{xy}.

At $\bar{M}$, a lower RS with a parabolic shape as a function of $\mathbf{k}_{||}$ was found. This state begins near the local gap located between -4.0 and -5.0 eV and ends in the middle of the $\bar{M}-\bar{\Gamma}$ interval. The wavefunction composition of this RS is $s, d_{x^2+y^2}$.

Near E_F at the $\bar{M}$ point, a surface state with a negative curvature is observed. The state goes into the local gap above E_F with a bandwidth of approximately 1.1 eV. The calculated wavefunction composition of this SS is $d_{x^2+y^2}$.

3.2.1. *Comparison with experiment*

It is well known that Pt(100) exhibits both the unreconstructed (1×1) surface and the reconstructed (5×1) surface [5-7]. However, the ideal surface was studied in this work, and the results will be compared with experimental data found for the (1$\times$ 1) phase.

Using angle–resolved photoemission spectroscopy Stampfl *et al.* [5] reported the SSs of Pt(100)(1$\times$1) at energies below E_F. These authors present a rich number of SSs along the $\bar{M}-\bar{\Gamma}-\bar{X}$ interval for the (1×1) phase (see Fig. 2 in Ref. 5). Although these states are not discussed in detail in Ref. 5, it will be shown that the general shape of the reported states is reproduced accurately in the present work.

As was reported by Stampfl *et al.* [5], there is an RS near E_F for the $\bar{M}-\bar{\Gamma}$ interval that follows the border of the E_F. The state shows almost zero dispersion as a function of $\mathbf{k}_{||}$ (see Fig. 2 in Ref. 5). The DFT calculations found a state around the $\bar{M}$ point located mainly in the local gap just above E_F, and this state could be identified with the experimental one.

There are two RSs reported at -0.6 and -0.9 eV at the $\bar{M}$ point. These states are dispersed throughout nearly the entire $\bar{M}-\bar{\Gamma}-\bar{X}$ interval (see Fig. 2 in Ref. 5). The energy dispersion of these states is worth noting and is reproduced properly in the DFT calculations (see Fig. 2). As mentioned above, these states show quasi–oscillatory behavior in this portion of the SBZ. A similar pattern can also be observed from the calculated bands shown in Fig. 2(b) in Ref. 5.

Stampfl *et al.* [5] reported another RS at low energies around -5.5 eV at the $\bar{M}$ point. This state is reproduced accurately in the DFT calculation as discussed above (see Fig. 2 and Table I).

TABLE I. Calculated energy values and wave function compositions of the different surface states found for Pt(100). The calculated ETB wave functions are also given for comparison. For details, see the discussion in the text.

Point	State	Energy value (eV)		Wave function	
		Experiment	Calculated	FLAPW	ETB
$\bar{\Gamma}$	SS	5.5 [7]	4.3	—	s, p_z
	RS	0.6 [7]			
	RS	–0.3 [5]	0.0	d_{xz}, d_{z^2}, d_{xy}	$d_{x^2+y^2}$
	RS	–6.5 [5]	–6.4	$s, d_{x^2+y^2}$	$d_{xy}, d_{3z^2-r^2}$
$\bar{X}$	SS		4.3	$s, d_{x^2+y^2}$	s, d_{xy}
	SS		2.1	—	p_x, p_y
	RS		0.0	d_{xz}, d_{z^2}	—
	RS	–2.5 [5]	–2.3	d_{xy}, d_{xz}	—
	RS	–4.0 [6]	–3.6	$d_{x^2+y^2}, d_{xz}$	d
	SS	–5.0[a]	–5.5	$s, d_{x^2+y^2}$	s, d_{xy}
$\bar{M}$	RS		9.0–10.0	d_{xy}	—
	SS	~ 0.0 [5]	1.1	$d_{x^2+y^2}$	—
	RS	–0.6 [5]	0.4	—	d_{xy}
	RS	–0.9 [5]	–0.6	d_{z^2}	—
	RS		–1.7	—	$d_{3z^2-r^2}$
	RS	–5.5 [5]	–5.2	$s, d_{x^2+y^2}$	—

[a] Value calculated by Benesh *et al*. [30].

Near the $\bar{X}$ point, an RS that reaches the $\bar{X}$ point was found around -2.3 eV. This state seems to be related to the state around –2.5 eV reported by Stampfl *et al.* [5].

Then, using angle–resolved photoemission spectroscopy Subaran *et al.* [6] reported a flat band around –4.0 eV at the $\bar{X}$ point, which differs from the experimental data reported in Ref. 5. It was speculated that this band represents emission from the surface layer or that it arises from absorbate atoms [6]. As was shown above, our calculations found an RS around -3.6 eV that accurately reproduces the dispersion and shape of the state reported by Subaran *et al.* [6]. As was mentioned there, this state seems to be part of a continuous band that crosses the entire SBZ (see Fig. 2 and Table I).

Stampfl *et al.* [5] reported another RS at energies around –6.5 eV at the $\bar{\Gamma}$ point. This state exhibits parabolic dispersion as a function of $\mathbf{k}_{||}$, and as mentioned above, our DFT calculations properly reproduce this state.

Stampfl *et al.* [5] reported an RS around –0.3 eV at the $\bar{\Gamma}$ point, and this state is also reproduced in the DFT calculations. Although we have found that this state is located at the maximum of the valence band (see Table I).

It is well known that it is difficult to reproduce experimental measurements individually. However, the accuracy of our calculated SSs and RSs in comparison with those reported by Stampfl *et al.* [5] for the Pt(100) surface is worth noting.

In an early experimental work Drube *et al.* [7] used angle–dependent inverse photoemission, to measure the SSs of Pt(100)(1×1) at energies above E_F. The energy band dispersion was found in the $\bar{\Gamma} - \bar{X}$ interval. The authors found an SS in the local gap above E_F, located at 5.5 eV, which was labeled S_1 in Fig. 3 of Ref. 7. They also report a state at 0.6 eV above E_F that seems to be an RS, the state labeled B_1 in Fig. 3 of Ref. 7. The authors also report a state labeled D. Drube *et al.* [7] mentioned that they did not find an explanation for this state. A state labeled B_2, which exhibited significant dispersion, was also reported. Although this state is found nearly inside the bulk bands, there is a portion of the state that penetrates into the local gap near the $\bar{X}$ point.

Discussion of these states and comparison with our DFT calculations is left for the next section, where the ETB results for the Pt(100) surface will be presented.

3.2.2. Tight–Binding Calculations

Figure 2 shows the calculated pbbs, SSs, and RSs for Pt(100) using the FLAPW method and compares them with those obtained using the ETB method. Table I shows the wavefunction compositions of the different SSs and RSs. As was found in our previous work for the Pt(111) case [4], the ETB calculation properly reproduces the pbbs, SSs, and RSs that were found in the DFT calculations. A few discrepancies are observed and will be discussed below. The observed differences include the fact that the ETB calculations do not find the same number of states that were found in the DFT calculations.

Figure 2 shows that the local energy gaps found in the ETB calculations are identical to those calculated using DFT. More importantly, the dispersion of the SSs in the local gaps found by the ETB calculations is almost the same as those found by the DFT calculations.

However, the ETB calculations predict an SS located in the local gap above E_F at the $\bar{\Gamma}$ point that seems to be related to the state S_1 reported by Drube *et al.* [7]. The state was not found in the DFT calculations. This SS was reported at approximately 5.5 eV, and in our ETB calculation the state was found at 4.3 eV. The state increases in energy to approximately 6.0 eV and seems to mix with the bulk bands. The calculated ETB wavefunction composition of this state exhibits s, p_z symmetry (see Table I).

Another SS was found in the ETB calculations but not in the DFT calculation. The state exhibits significant dispersion as a function of $\mathbf{k}_{||}$, it is located at approximately 2.1 eV in the local gap around the $\bar{X}$ point, and disperses following the lower edge of the local gap. The calculated ETB wavefunction composition of this state has the p_x, p_y symmetry (see Table I).

An SS following the upper edge of the local gap at $\bar{X}$ was found at approximately 4.3 eV. It was found that both calculations predict this state, but no experimental evidence for this state was found.

At energies below E_F, the ETB calculation properly reproduces most of the SSs and RSs found in the DFT calculations, as it is shown in Fig. 2. In some cases, there are some small numerical differences in the calculated energy values of these states, but in general, most of the features found in the DFT calculation were also found in the ETB calculation.

The ETB calculations also reproduce most of the experimental data reported by Stampfl *et al.* [5] (see Table I). These facts demonstrate the predictive power of the ETB method.

3.3. Platinum(110)

Figure 3 shows the calculated pbbs, SSs, and RSs for Pt(110). Table II shows the calculated wavefunction compositions of the different SSs and RSs of this surface.

As in a previous case, the figure shows the pbbs as small black dots, and the SSs and RSs are shown as red dots. The figure shows four local gaps above E_F, and three local gaps are found at energies below E_F.

From our calculations, three SSs above E_F were found. An SS is found in the local gap at the $\bar{X}$ point around 5.3 eV. This state exhibits nearly parabolic behavior as a function of $\mathbf{k}_{||}$, and its energy bandwidth is approximately 1.0 eV. The state mixes with a calculated RS obtained at the $\bar{S}-$point at approximately 6.2 eV. The wavefunction of this SS has s, p_z symmetry.

Another SS was located near the bottom of this local gap. This state is located at 2.4 eV and extends a few $k-$values from the $\bar{X}$ point. The computed wavefunction composition of this state is $s, d_{x^2+y^2}, d_{xz}$.

Near the $\bar{X}$ point, there is an RS that should be noted. This state shows peculiar behavior as a function of $\mathbf{k}_{||}$. The state seems to originate in the group of RSs located in the energy range from 0 to 1.0 eV below E_F and exhibits significant energy dispersion following the edge of the local gap.

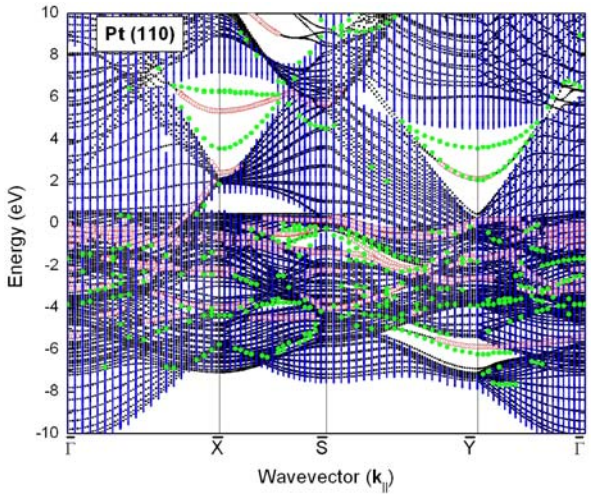

FIGURE 3. (Color online) Projected bulk bands of Pt(110). The black dots represent the DFT calculated pbbs. Red dots represent SSs or RSs if the states are located in a local energy gap or in the continuum bulk bands, respectively. The blue dots represent the pbbs calculated using the ETB method, and the SSs and RSs are represented by green dots.

An SS was obtained in the local gap at the $\bar{Y}$ point. This state exhibits little dispersion as a function of $\mathbf{k}_{||}$. The state is located at approximately 2.1 eV, and the calculated wavefunction composition of this state is $s, d_{x^2+y^2}, d_{xz}$.

As for the previous surface, a number of RSs were found at energies below E_F and are shown in Fig. 3. The main characteristics of these states are as follows:

A noticeable SS was found at low energies, approximately -5.9 eV in the $\bar{Y}-\bar{\Gamma}$ interval. The state begins in the lower local gap at $\bar{Y}$ and then continues into the continuum of the pbbs in the $\bar{Y}-\bar{\Gamma}$ interval. The wavefunction composition of this state is $s, d_{x^2+y^2}$.

Similarly, a series of RSs were found near E_F in the $\bar{Y}-\bar{\Gamma}$ interval located at energies that range from 0.0 to –3.0 eV. The states then go through the $\bar{\Gamma}-\bar{X}$ interval.

At energies near E_F, around 0.1 eV at the $\bar{S}$ point, an RS was found that follows the dispersion of the upper pbbs. This state extends from the middle of the $\bar{X}-\bar{S}$ through the $\bar{S}-\bar{Y}$ intervals. This state is a hybridization of the $s, d_{x^2+y^2}, d_{xy}$ orbitals.

A series of RSs were found at the $\bar{X}$ point. There is one RS around –0.7 eV that seems to be part of the states coming from the $\bar{\Gamma}-\bar{X}$ interval and going to the $\bar{S}$ point and then to the $\bar{Y}$ point. The wavefunction composition of this state is s, d_{yz}, d_{z^2}. Another RS is located around -2.1 eV. An RS located at approximately -4.2 eV was also found. The wavefunction compositions of these states primarily have the symmetries of the d_{xz} and s, d_{xy} orbitals, respectively.

A local gap at –0.5 eV is observed at the $\bar{S}$ point, and an SS is located there. The wavefunction composition of this state is primarily d_{yz}. The already mentioned SS at –1.4 eV was also found at this point and its wavefunction composition is d_{xz}, d_{z^2}. Other RS with a parabolic shape is located

TABLE II. Calculated energy values and wave function compositions of the different surface states for Pt(110). For comparison, the calculated ETB wave functions are also given. For details, see the discussion in the text.

Point	State	Energy value (eV)		Wave function	
		Experiment	Calculated	FLAPW	ETB
$\bar{\Gamma}$	SS		6.9	—	s, p_x, p_y
	RS	5.0 [8]			
	RS	3.0 [8]			
	RS	0.4 [8]			
	RS		$0 \rightarrow -1.2$	d_{yz}, d_{z^2}	—
	RS		–1.7	—	$d_{yz}, d_{x^2+y^2}$
$\bar{X}$	SS		6.2	—	s, p_z
	SS	6.0 [8]	5.3	s, p_z	—
	SS		3.6	—	p_x
	SS		2.4	$s, d_{x^2+y^2}, d_{xz}$	—
	RS		–0.7	s, d_{xy}, d_{z^2}	—
	RS		–2.1	d_{xz}	—
	RS		–4.2	s, d_{xy}	—
	RS		–5.7	—	p_x, d_{xy}, d_{yz}
$\bar{S}$	RS		4.5	—	d
	RS	~ 0.0 [10]	0.1	$s, d_{x^2+y^2}, d_{xy}$	—
	SS		–0.5	d_{xz}	—
	SS		–1.4	d_{xz}, d_{z^2}	—
	RS		–2.2	$d_{x^2+y^2}$	—
	RS		–4.0	d_{xy}	—
	RS		–4.5	s, d_{xy}	—
	RS		–5.2	—	d_{xz}
$\bar{Y}$	SS	5.1 [8]	3.6	—	s, p_z
	SS	1.3 [8]	2.1	$s, d_{x^2+y^2}, d_{xz}$	p_y, d_{yz}
	RS		–3.9	—	$d_{yz}, d_{x^2+y^2}$
	RS		–5.9	$s, d_{x^2+y^2}$	$s, p_z, d_{x^2+y^2}, d_{3z^2-r^2}$

around –2.2 eV and has the wavefunction composition $d_{x^2+y^2}$. An RS around –4.0 eV was also found. The wavefunction composition of this state has the d_{xy} symmetry. The final RS is located in the $\bar{X} - \bar{S}$ interval around –4.5 eV. The wavefunction of this state has s, d_{xy} symmetry.

3.3.1. Comparison with experiment

For energies above E_F, experimental reports of the electronic band structure of this surface can be found [8,9]. To our knowledge, however, no studies of the electronic band structure for this surface at energies below E_F have been published.

It is well established that Pt(110) exhibits a reconstruction called (2×1) missing row [8-10]. Because an ideal surface calculation was performed here, it is not possible to compare quantitatively the results with the measured values. However, the experimental results will be used as a guide to discuss our calculations.

In a recent inverse photoemission (IPE) spectroscopy experiment, Memmel *et al.* [8,9] presented a series of SSs and RSs for the $\bar{X} - \bar{\Gamma} - \bar{Y}$ interval. It is interesting to note that in the local gap at the $\bar{X}$ point, Memmel *et al.* [8] report an SS at approximately 6.0 eV (labeled S_0^+ in Fig. 3 of Ref. 8), which is found to be a one–dimensional state. This result means that the state is insensitive to the (1×2) missing row reconstruction [8,9]. The one–dimensional character of this state is the reason that our calculations accurately reproduce this state. However, the calculated SS shows more dispersion than the measured state, and in our calculations the state is predicted at 5.3 eV.

As mentioned above, a lower local gap was also calculated at $\bar{X}$. The calculations predict that this lower local gap has an energy width of almost 1.5 eV, whereas the experi-

mental study reports a gap with an energy width of almost 1.0 eV.

At the same time, the calculations predict an RS that exhibits significant dispersion along the edge of the lower local gap, whereas the experimental study presents an RS following the edge of the upper local gap.

In the local gap at the $\bar{Y}$ point, Memmel *et al.* [8] report an SS at an energy of 1.3 eV along with other weak features that should be identified with umklapp processes from the $\bar{\Gamma}$ point [8]. The DFT calculations found an SS near the lower edge of this local gap, at approximately 2.1 eV.

At the upper energies, Memmel *et al.* [8] report a flat SS at 5.1 eV, labeled S_0^+ in Fig. 3 of Ref. 8. However, the DFT calculations do not reproduce this state.

Just above E_F in the rest of the SBZ, Memmel *et al.* [8] report several states mixed with the pbbs. The flat state at E_F in the $\bar{X}-\bar{\Gamma}-\bar{Y}$ interval, which should represent an RS, should be noted. There is also a state labeled C that shows a negative slope centered at $\bar{\Gamma}$, around 3.0 eV. Finally, there are a series of states around 1.0 eV at $\bar{\Gamma}$, shown in Fig. 3 of Ref. 8, as well as a state labeled IS around 5.0 eV at $\bar{\Gamma}$.

The DFT calculations do not reproduce these states in detail. However, a series of states was found near E_F that show little dispersion as functions of $\mathbf{k}_{||}$ and covered the $\bar{S}\bar{Y}$ interval (see also the above discussion related to Fig. 3).

As discussed above, a number of SSs and RSs were found at energies below E_F. However, because we did not find enough experimental data in this energy region, we only comment on our results for the RS near E_F at the $\bar{S}$ point, and further commentaries on the rest of the states will be omitted.

The RS at 0.0 eV around the $\bar{S}$ point was previously discussed by Menzel *et al.* [10]. These authors mentioned that this state is observed in clean Pt(110) surfaces as well as in the Br/Pt(110)$-c(2\times 2)$ system. In a related work, Minca *et al.* [11] also discuss an RS at the $\bar{X}$ point. The authors mention that this state appears because the bulk energy bands present a flat band along the WLW line just below E_F. This band creates a van Hove singularity at E_F. The bulk band, when projected onto the $\bar{S}$ point of the (110) SBZ, is the origin of the observed resonance state. The results obtained for the ideal Pt(110) surface show that the RS at the $\bar{S}$ point is a characteristic of this surface and is independent of the reconstruction. Similar observations were noted for the one–dimensional SS at the $\bar{X}$ point above E_F, as described by Memmel *et al.* [8].

3.3.2. Tight-Binding Calculation

Figure 3 shows the pbbs, SSs, and RSs for the Pt(110) ideal surface found using the ETB method. In the figure, the blue (black) dots represent the pbbs calculated using the ETB (FLAPW) method, while the green (red) dots represent the SSs and RSs calculated using the ETB (FLAPW) method. There are small differences at the edges of the calculated local gaps above E_F, however, at energies below E_F the calculated pbbs are similar in both methods. For details, see the figure caption.

At energies above E_F, a series of SSs were found, and will be discussed in detail in the rest of the section. As mentioned above, an SS around 5.3 eV was found at the $\bar{X}$ point in the DFT calculation. In the ETB calculation, however, an SS with a quasi–linear shape as a function of $\mathbf{k}_{||}$ was found at approximately 6.2 eV. Although this SS has different energies in the two calculations, the wavefunction symmetries found by the two methods are the same (see Table II). The state also shows the trend reported by Memmel *et al.* [8] for the S_0^+ state.

The ETB calculation predicts a second SS around 3.6 eV at the $\bar{X}$ point near the lower edge of the local gap. This state differs in its energy, although not in its shape, from the state found at 2.4 eV in the DFT calculation. The wavefunction composition of this state shows the p_z symmetry.

The ETB calculation predicts an RS at approximately 4.5 eV near the $\bar{S}$ point. The wavefunction composition of this state has the full d symmetry. The ETB calculation shows that an RS was found in the upper energies around the local gap at the $\bar{S}$ point, around 9.5 eV. However, no experimental evidence for this state was found. The same is true of the SS calculated using the FLAPW method, which was located in the upper local gap near the $\bar{S}$ point at approximately 9.0 eV.

Two SSs were found in the local gap around the $\bar{Y}$ point. The lower state follows the dispersion found in the DFT calculation, and the state extends over the entire local gap. The ETB calculation predicts an upper SS around 3.6 eV that was not found in the DFT calculation. This state could be related to the state reported by Memmel *et al.* [8] at these energies. To support this speculation, however, it is necessary to assume that this SS is independent of the missing row reconstruction. The wavefunction composition of these states has the s, p_z and p_y, d_{yz} symmetry, respectively.

At energies below E_F, the calculated SSs in the main local gaps were accurately reproduced in both calculations. For example, the ETB calculation found an SS around -0.5 eV in the local gap at the $\bar{S}$ point with noticeable dispersion, in agreement with the state calculated using the FLAPW method.

In the lower local gap at $\bar{Y}$, the SS found around -6.2 eV in the ETB calculation exhibits nearly the same dispersion as the state found at -5.9 eV using the FLAPW method.

On the other hand, Fig. 3 shows that a number of RSs were obtained from the ETB calculations. However, most of these RSs do not match any states calculated using the FLAPW method. In this case, the two calculations provide us with different series of RSs, contrary to what was obtained for the Pt(100) surface (see Fig. 2). A possible explanation of these results could be the need to include reconstruction effects in the calculations.

Finally, for the above E_F energies, when compared with the experimental data the ETB calculation properly predicts the SSs found in the local gaps. Because the calculations in this work were done for an ideal surface, some differences

in the energies values were observed. Nevertheless, these findings demonstrate the predictive power of the ETB calculations compared with the more computationally demanding methods. In this sense, the two methods complement each other.

4. Conclusions

We have calculated the electronic band structure of platinum low–index surfaces. In our calculations, we used both DFT and empirical methods. From our calculations, we report the pbbs, SSs, and RSs for ideal Pt(100) and Pt(110) surfaces. Comparisons with experimental data show that our calculations properly predict the SSs and RSs for Pt(100) surfaces. Because the Pt(110) surface exhibits the so–called (2×1) missing row reconstruction that was not included in our calculations, our results compare poorly with the SSs reported for this surface. However, when the reported SSs are independent of the reconstruction, we found that our calculations properly reproduce the experimental states. The results of our calculations for ideal surfaces demonstrate the predictive power of the empirical method.

1. A. Stroppa, K. Termentzidis, J. Paier, G. Kresse, and J. Hafner, *Phys. Rev. B* **76** (2007) 195440; A. Stroppa and G. Kresse, *New J. Phys.* **10** (2008) 063020; L. Schimka, J. Harl, A. Stroppa, A. Grüneis, M. Marsman, F. Mittendorfer, and G. Kresse, *Nature Materials* **9** (2010) 741-744.
2. P. Roos, E. Bertel, and K.D. Rendulic, *Chem. Phys. Lett.* **232** (1992) 537.
3. S. Baud, C. Ramseyer, G. Bihlmayer, S. Blügel, C. Barreteau, M.C. Desjonquères, D. Spanjaard, and N. Bernstein, *Phys. Rev. B* **70** (2004) 235423.
4. H.J. Herrera–Suárez, A. Rubio–Ponce, and D. Olguín, (to be published in Comp. Mat. Scie.)
5. A.P.J. Stampfl, R. Martin, P. Garner, and A.M. Bradshaw, *Phys. Rev. B* **51** (1995) 10197.
6. W. Subaran, H. Nakajima, A. Kakizaki, and T. Ishii, *J. Elec. Spec. and Related Phenom.* **144–147** (2005) 613.
7. R. Drube, V. Dose and A. Goldmann, *Surf. Scie.* **197** (1988) 317.
8. N. Memmel, G. Rangelov, and WE. Bertel, *Prog. Surf. Scie.* **74** (2003) 239.
9. G. Rangelov and V. Dose, *Bulg. Chem. Comm.* **26** (1993) 159.
10. A. Menzel, Zh. Zhang, M. Minca, Th. Loerting, C. Deisl, and E. Bertel, *New J. Phys.* **7** (2005) 102.
11. M. Minca, S. Penner, E. Dona, A. Menzel, E. Bertel, V. Brouet, and J. Redinger, *New J. Phys.* **9** (2007) 386; A. Menzel, Z. Zhang, M. Minca, E. Bertel, J. Redinger, R. Zucca, *J. Phys. Chem. Solids* **67** (2006) 254;
12. P. Blaha, K. Schwarz, G.K.H. Madsen, D. Kvasnicka, and J. Luitz, *WIEN2k, An Augmented Plane Wave Plus Local Orbitals Program for Calculating Crystal Properties*, ISBN 3-9501031-1-2, (Vienna University of Technology, Austria, 2001).
13. L. Vitos, A.V. Ruban, H.L. Skriver, and J. Kollár, *Surf. Scie.* **411** (1998) 186.
14. F.D. Murnaghan, *Proc. Nat. Acad. Sci. U.S.A.* **30** (1944) 244; F. Birch, *Phys. Rev.* **71** (1947) 809.
15. Landolt–Börstein, Numerical Data and Functional Relationships in Science and Technology *New Series:* Group III: Solid State Physics, Volume 24, Physics of Solid Surfaces, Subvolume a, Structure. Editor: G. Chianrotti, Springer–Verlag, Berlin, Heidelberg, New York, London, Paris, Tokyo, Hong Kong, Barcelona, Budapest, (1993).
16. C. Kittel, *Introduction to Solid State Physics, Eighth Edition*, (John Wiley & Sons Inc., 2005).
17. H.J. Monkhorst and J.D. Pack, *Phys. Rev. B* **13** (1976) 5188.
18. J.C. Slater and G.F. Koster, *Phys. Rev.* **94** (1954) 1498.
19. D.A. Papaconstantopoulos, *Handbook of the Band Structure of Elemental Solids* (Pleunm, New York, 1986).
20. F. García-Moliner, V. Velasco, *Theory of Single and Multiple Interfaces* (World Scientific, 1992); F. García–Moliner and V. Velasco, *Prog. Surf. Sci.* **21** (1986) 93.
21. L. Falicov and F. Yndurain, *J. Phys. C: Solid St. Phys.* **8** (1975) 147.
22. M.P. López–Sancho, J.M. López–Sancho, and J. Rubio, *J. Phys. C: Metal Phys.* **14** (1984) 1205; **15** (185) 855.
23. F. Rodríguez, A. Camacho, and R. Baquero, *Phys. Status Solidi B* **160** (1990) 127; R. Baquero, V.R. Velasco, and F. García–Moliner, *Phys. Scr.* **38** (1988) 742; R. Baquero and A. Noguera, *Rev. Mex. Fis.* **35** (1989) 638.
24. D. Olguín and R. Baquero, *Phys. Rev. B* **51** (1995) 16981; D. Olguín and R. Baquero, *Phys. Rev. B* **50** (1994) 1980; D. Olguín, J.A. Rodríguez, and R. Baquero, *Europ. Phys. J. B* **32** (2003) 119.
25. R. Baquero and A. Noguera, *Rev. Mex. Fis.* **35** (1989) 638.
26. L.M. García–Cruz *et al.*, *Can. J. of Physics* **82** (2004) 717; A. Rubio-Ponce, A.E. García, and R. Baquero, *Rev. Mex. Fis.* **49** (2003) 411; L.M. García–Cruz, A.V. Gaftoi, A. Rubio-Ponce, A.E. , García, and R. Baquero, *Phys. Status Solidi B* **220** (2000) 449.
27. R. Baquero and R. de Coss, *Phys. Status Solidi B* **169** (1992) K69–K71; R. de Coss and R. Baquero, *Rev. Mex. de Fis.* **41** (1995) 875; R. de Coss, *Phys. Rev. B* **52** (1995) 4768; R. de Coss, *Surf. Rev. and Lett.* **3** (1996) 1505.
28. R. Baquero, A. Noguera, A. Camacho, and L. Quiroga, *Phys. Rev. B* **42** (1990) 7006.
29. C. Quintanar, R. Baquero, V.R. Velasco and F. García–Moliner, *Rev. Mex. Fis.* **37** (1991) 503.
30. G.A. Benesh, L.S.G. Liyanage, and J.C. Oingel, *J. Phys. Condens. Matt.* **2** (1990) 9065.